Unlocking the potential of organ-on-chip models through pumpless and tubeless microfluidics

AUTHOR(S)

L C Delon, Azadeh Nilghaz, E Cheah, C Prestidge, B Thierry

PUBLICATION DATE

01-06-2020

HANDLE

10536/DRO/DU:30138194

ADVANCED HEALTHCARE MATERIALS
www.advhealthmat.de

Unlocking the Potential of Organ-on-Chip Models through Pumpless and Tubeless Microfluidics

*Ludivine C. Delon, Azadeh Nilghaz, Edward Cheah, Clive Prestidge, and Benjamin Thierry**

Microfluidic organs-on-chips are rapidly being developed toward eliminating the shortcomings of static in vitro models and better addressing basic and translational research questions. A critical aspect is the dynamic culture environment they provide. However, the associated inherent requirement for controlled fluid shear stress (FSS) and therefore the need for precise pumps limits their implementation. To address this issue, here a novel approach to manufacture pumpless and tubeless organs-on-chips is reported. It relies on the use of a hydrophilic thread to provide a driving force for the perfusion of the cell culture medium through constant evaporation in the controlled conditions of a cell incubator. Well-defined and tuneable flow rates can be applied by adjusting the length and/or diameter of the thread. This approach for the preparation of an intestine-on-chip model based on the Caco-2 cell line is validated. Five days culture under 0.02 dyn·cm^{-2} shear conditions yield monolayers similar to those prepared using a high-precision peristaltic pump. A pumpless device can also be used to delineate the effect of FSS on the phenotype of adenocarcinomic human alveolar basal epithelial A549 cells. It is anticipated that the pumpless approach will facilitate and herefore increase the use of organs-on-chips models in the future.

1. Introduction

Microfluidic cell culture technology, often referred to as organs-on-chips, is rapidly progressing and promises to allow the preparation of in vitro models that better recapitulate the key structural and functional aspects of human tissues, and consequently that are more physiologically relevant.[1] A key feature of organs-on-chips models is the application of dynamic culture environments that directly influence the phenotype and behavior of living cells and tissues, including their proliferation, differentiation, and migration.[2] This is not surprising as fluid shear stress (FSS) has been shown previously to have an important effect not only on endothelial cells[3] but more generally on epithelial cells,[4,5] cultured in vitro. Several organs-on-chips models are now well established and commonly used, including lung,[6] intestine,[7] and liver[8] on-chip, and their application is broadly anticipated to yield new knowledge and/or assist in the development of novel therapeutic approaches.

Most of the organs-on-chips technologies developed to date require the use of an external pump connected to the device through tubing to enable the perfusion of cell culture medium and buffer within the microfluidic channels.[9] This configuration is a bottleneck in the application of organs-on-chips in laboratories with no experience in microfluidic technologies. It is inherently prone to the formation of bubbles and/or leakages within these microfluidic organs-on-chips devices, which creates uncontrolled culture conditions and therefore compromises the experiment. In addition, this configuration is also associated with specific biosafety issues for applications requiring the use of biologically hazardous agents such as pathogens or viruses. Finally, the requirement for high-precision pumps increases the initial capital cost required to establish organs-on-chips.

To address these issues, alternative methods have been recently proposed to eliminate the need for external pumps and tubing. These include the application of hydrostatic pressure and resistance circuit,[10] gravity-induced bidirectional flow (rocking platform),[11–14] or modification of the gravity-driven siphon flow using an intravenous infusion set.[15] Despite their merits, these methods all have significant drawbacks in the context of organs-on-chips. Devices based on in-built hydrostatic pressure have limited flexibility in regard to modulating the flow conditions and do not allow rapid exchange of the culture medium, for example, to expose the cells to drugs. Rocking platforms create inhomogeneous complex flow conditions and therefore shear stresses, and remain expensive to implement. Simpler perfusion systems need to be developed to encourage and facilitate the use of organs-on-chips by non-microfluidic users.

To address this need, we demonstrate a simple yet robust approach to fabricate pumpless organs-on-chips devices. It is based on the introduction of a hydrophilic thread in the outlet of the microfluidic circuit (**Figure 1**). The ability of hydrophilic

L. C. Delon, Dr. A. Nilghaz, E. Cheah, Prof. B. Thierry
Future Industries Institute and ARC Centre of Excellence Convergent Bio-Nano Science and Technology
University of South Australia
Mawson Lakes Campus, Adelaide, SA 5095, Australia
E-mail: Benjamin.Thierry@unisa.edu.au
L. C. Delon, Prof. C. Prestidge, Prof. B. Thierry
School of Pharmacy and Medical Sciences and ARC Centre of Excellence Convergent Bio-Nano Science and Technology
University of South Australia
City West Campus Adelaide, SA 5000, Australia

The ORCID identification number(s) for the author(s) of this article can be found under https://doi.org/10.1002/adhm.201901784

DOI: 10.1002/adhm.201901784

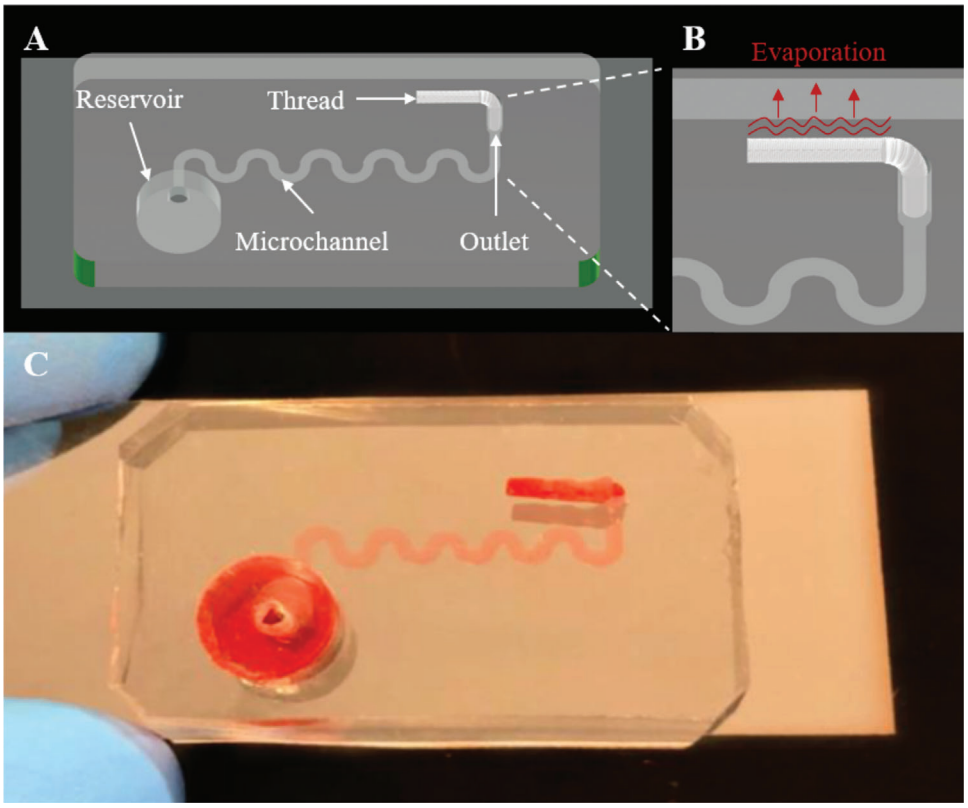

Figure 1. A,B) Schematic illustration of the pumpless organ-on-chip device. The flow in the device is driven by constant evaporation of cell culture medium wicked by the superhydrophilic thread inserted in the outlet. C) Photograph of a constant-width polydimethylsiloxane (PDMS) device mounted on a coverslip.

threads to serve as microfluidic capillary channels has been actively exploited to design lab-on-chip bioassay, but we demonstrate here their application in the field of organs-on-chips for the first time. Constant evaporation of the culture medium wicked by the threads in the controlled environment of a cell culture incubator (typically 37 °C, 5% CO_2, and 90% humidity) provides a reliable driving force to achieve continuous flow of the culture medium over 24 h without the requirement for either a pump, external power source, or tubing.[16] Importantly, this approach is highly flexible and allows to readily tune the flow rate within the device, hence the shear stress experienced by cellular monolayers, simply by adjusting the length and/or diameter of the thread. It is also straightforward to inject medium/buffer to flush the cellular monolayer, for example, to expose it to a drug. We demonstrate the relevance and efficiency of the method by culturing two cell lines commonly used in organs-on-chips applications, namely Caco-2 and A549 cells, in microfluidic organs-on-chips models with different designs.

2. Results and Discussion

2.1. Characterization of Thread-Driven Flows within Microfluidic Devices

Non-woven Spunlace threads are commonly used in a broad range of medical products such as wound dressing and available in different diameters. They were therefore selected for this application. The Spunlace thread structure is shown in **Figure 2**A,B by scanning electron microscope (SEM) images. Such threads are ready-to-use microfluidic channels made of twisted fibers and form capillary channels that wick aqueous solution from the wet sections of the thread to the dry ones. The fibers consisting the Spunlace thread used here displayed smooth surfaces and diameters of ≈15 µm as shown by SEM. Pieces of wax and other impurities can be seen on the images of the as-received threads. Such impurities can be easily removed by plasma oxidation or mercerization, which in turn makes the threads more hydrophilic. The capillary rise in Spunlace threads was first characterized by measuring the wicking height of a dye solution at different time points for threads with four different diameters (Figure 2C). These measurements confirmed the feasibility of tuning the wicking rates of threads by simply tuning their dimensions.

Next, we endeavored to demonstrate the feasibility of using the constant evaporation of the medium wicked by a thread inserted within the outlet of a microfluidic device to accurately drive the flow within. To ensure the channels never dries out during an experiment, the placement of the thread can be adjusted so that it does not touch the bottom of the channel. This simple trick interrupts the wicking of the cell culture medium before emptying out the main channel in the situation where the inlet reservoir has not been refilled. While manual placement of the thread within the outlet can be carried out, this should be done carefully to ensure that is correctly positioned. We envisage that a lid

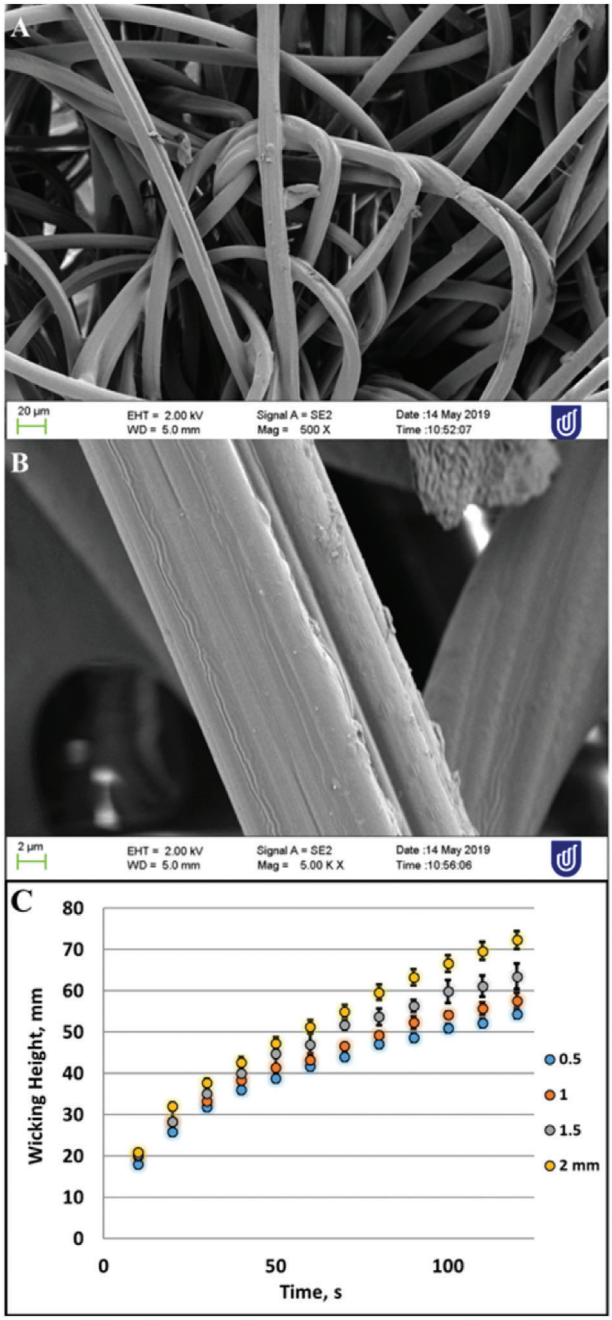

Figure 2. A,B) Structure of a superhydrophilic thread shown by electron microscopy at different magnifications. C) Capillary rise measurement of superhydrophilic threads (0.5, 1, 1.5, and 2 mm diameter threads were tested).

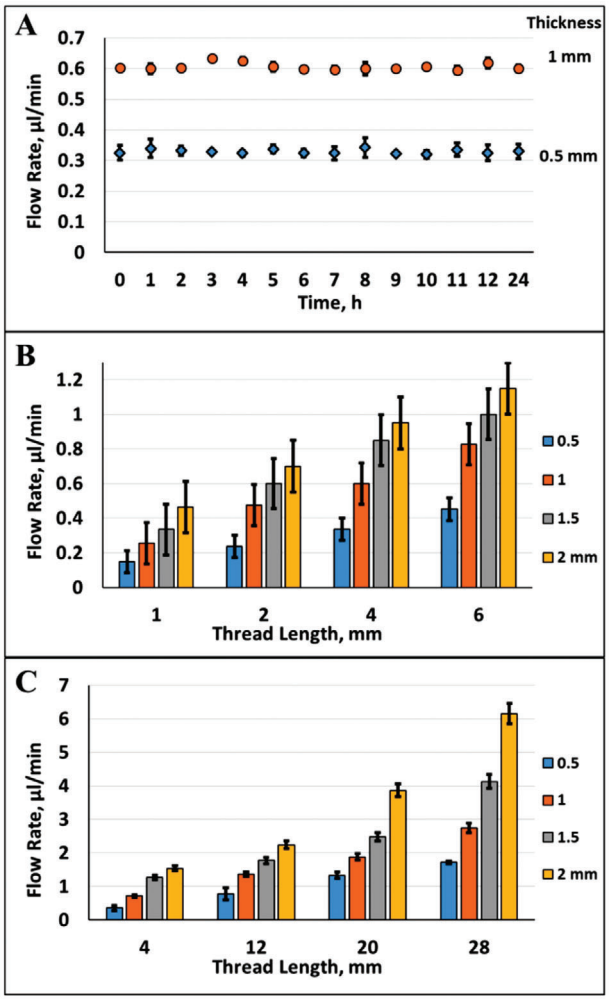

Figure 3. A) Stability over 24 h of the flow rates driven by threads with diameters of 0.5 and 1 mm. B,C) Flow rates versus thread characteristic dimensions, for the low flow rate range (B, thread straight) and high flow rate range (C, thread bent alongside the device).

comprising the thread could be used to ensure the accurate placement of the thread.

The flow rate in a constant-width device (with dimensions of 1 mm in width and 150 µm in height) induced by a thread was measured by tracking the displacement of highly fluorescent polystyrene 200 nm beads (see videos in the Supporting Information SI1). These measurements are shown in **Figure 3** and confirmed that the constant evaporation of a thread wicking the outlet of a microfluidic channel generates constant velocity over up to 24 h and therefore flow of the culture medium over time (Figure 3A). Importantly, changing the length of the thread as well as its diameter allowed to efficiently control the two key parameters driving the flow, namely the evaporation of the medium and rate of wicking, respectively (Figure 3B). Longer threads were found to be too heavy when wetted by the buffer/medium and collapse alongside the device. On the other hand, short threads remained orthogonal to the device, presenting a slightly different configuration as indicated in Figure 3. The flow rates induced by the various threads were measured, demonstrating the possibility of readily tuning rates from 0.15 µL min^{-1} (thread diameter of 0.5 mm and length of 1 mm) to 6 µL min^{-1} (thread diameter of 2 mm and length of 28 mm). Based on these measurements, we identified the most suitable thread length and diameter for a specific organ-on-chip device and cell type (**Table 1**). It should be noted that depending of the characteristic dimensions of the thread and the experimental conditions, including the medium/buffer composition and evaporation rate, the

Table 1. Flow rates and shear stresses τ_{cell} used in the devices for Caco-2 and A549 cell lines.

Device	Caco-2 cells		A 549 cells	
	Constant width	Hele-Shaw	Constant width	Hele-Shaw
Flow rates	0.15 µL min^{-1}	0.22 µL min^{-1}	0.6 µL min^{-1}	1 µL min^{-1}
Fluid shear Stresses	0.02 dyn cm^{-2}	From 0.03–0.002 dyn cm^{-2}	0.15 dyn cm^{-2}	From 0.135–0.008 dyn cm^{-2}
Thread dimensions	Length 1 mm, diameter 0.5 mm	Length 5 mm, diameter 1 mm	Length 4 mm, diameter 1 mm	Length 12 mm, diameter 1 mm

Caco-2 cell monolayers cultured within pumpless devices were compared to monolayers prepared in devices perfused by a peristaltic pump (Langer Instruments, USA). Note that although the overall flow rates were kept identical, monolayers grown in the pump-driven devices experienced peristatic flow while monolayers grown in pumpless devices experienced constant flow.

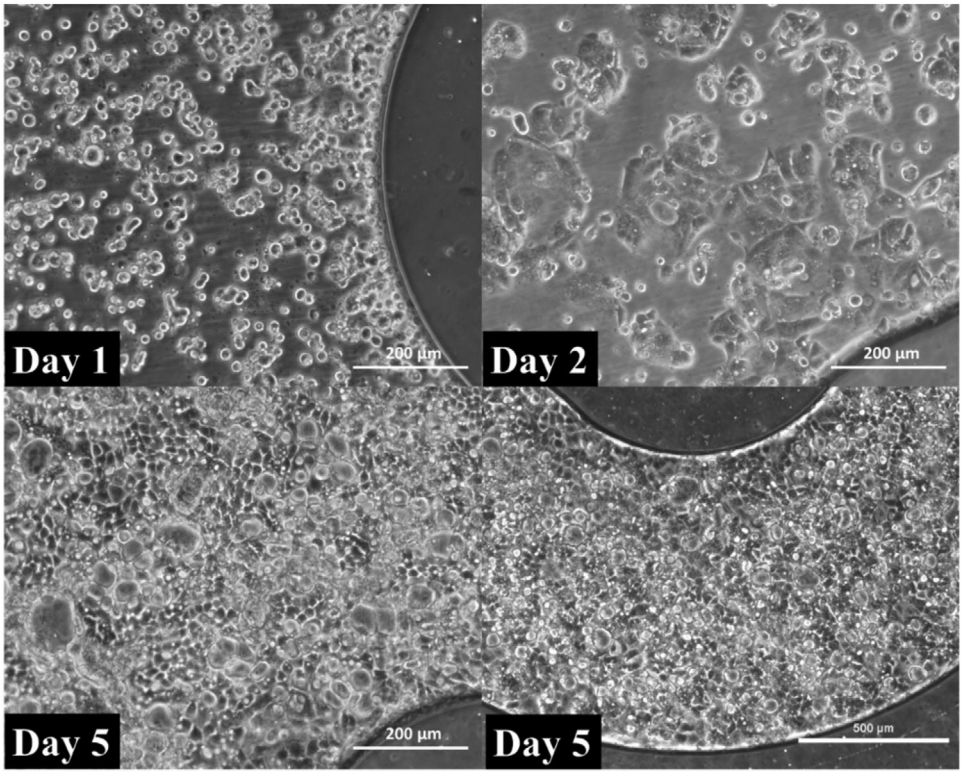

Figure 4. Bright field images of Caco-2 cells cultured in the constant-width pumpless device from day 1 to day 5 under a fluid shear stress τ_{cell} = 0.02 dyn cm^{-2}.

utilization of a new thread will be required to maintain a constant flow within the device as the evaporation of the media containing salts and biomolecules will ultimately clog the thread. In the experimental conditions used in this work, a single thread could be used over the 5 days required to obtain a differentiated monolayer.

2.2. Pumpless Culture of Caco-2 Cell Monolayers

The Caco-2 cell line is the most commonly used in vitro model of the intestinal barrier, including in the context of intestine-on-chip models. We have previously demonstrated the importance of tuning the microfluidic culture condition of Caco-2 cells monolayers and more specifically the applied FSS induced by the culture medium flow within microfluidic channels using a peristaltic pump.[4] We therefore next endeavored to demonstrate that pumpless culture of Caco-2 cell monolayers using thread-driven flow generates monolayers displaying structure, functions, hence phenotype similar to those cultured using an external pump. **Figure 4** depicts the growth of Caco-2 cells seeded within the constant-width microfluidic device. Cells were seeded at a density of 2×10^5 cells cm^{-2} and left to adhere to the Matrigel coated coverslip overnight. A thread of suitable dimensions was then inserted in the outlet to initiate flow of the culture medium from the inlet reservoir. Bright field images were then regularly acquired to monitor the formation of a confluent monolayer in the device. A similar experiment was performed in the Hele-Shaw device (see Figures S1 and S2, Supporting Information 2 (SI2)). Sections of the Hele-Shaw device were arbitrarily created along the z axis,

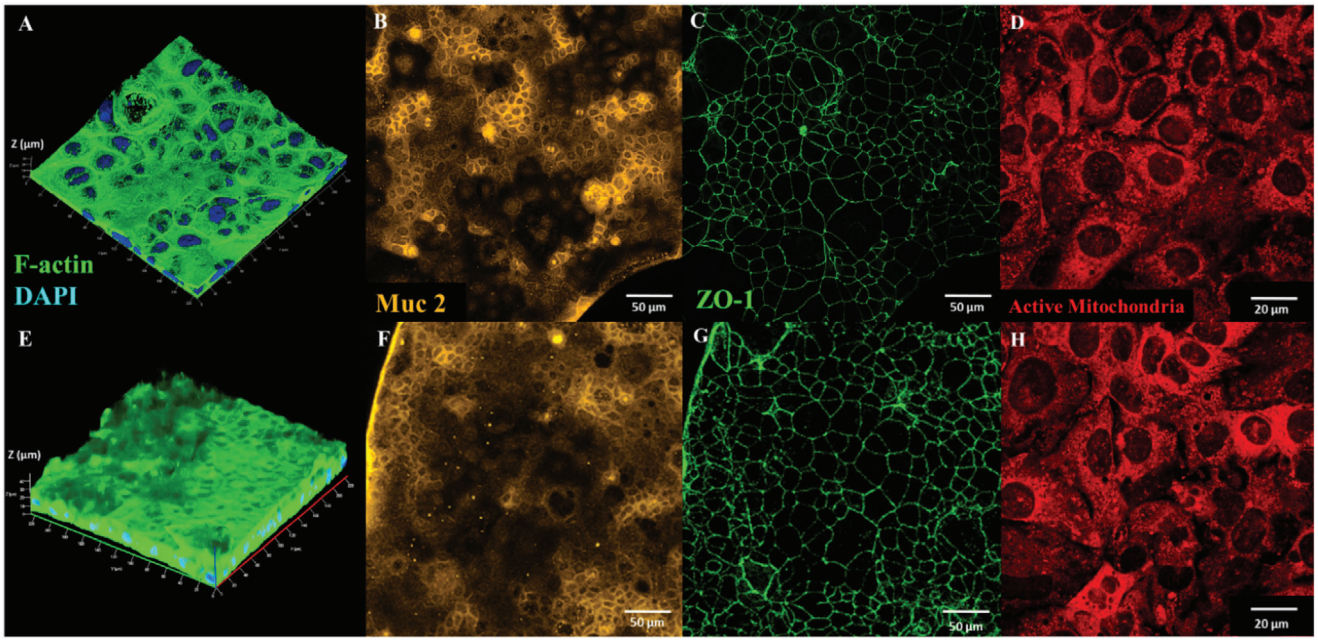

Figure 5. Caco-2 cells differentiation A–D) in a pumpless device versus E–H) in a device with peristaltic pump. F-actin network (green; A,E); production of mucin 2 (yellow; B,F); tight junctions protein ZO-1 expression (green; C,G); presence of active mitochondria (red; D,H).

corresponding to well-defined ranges of applied FSS experienced by the cells (τ_{cell} ranging from 0.03 to 0.002 dyn cm^{-2}). Confluent monolayers were formed at day 5 in all sections of the devices as well as for cells seeded in constant-width devices. Next, we investigated the characteristics of the Caco-2 cell monolayers obtained after 5 days of pumpless dynamic culture ($\tau_{cell} = 0.02$ dyn cm^{-2}). Caco-2 cells monolayers displayed a dense F-actin network (**Figure 5**A), high level of tight junctions (ZO-1 protein expression shown in Figure 5C), and high numbers of active mitochondria (Figure 5D). These observations are in excellent agreement with Caco-2 monolayers cultured under an identical FSS applied using an external pump[4,20,23] (Figure 5) and demonstrates that efficient differentiation occurs within 5 days of culture in the pumpless device.

2.3. Pumpless Culture of A549 Cell Monolayers

Having demonstrated the feasibility of using thread-driven flow to culture cells within microfluidic organs-on-chips devices, we next aimed to illustrate the utility of this approach to delineate the phenotypical changes occurring in A549 cells in response to the applied FSS. It has been demonstrated that the adenocarcinomic human alveolar basal epithelial A549 cells undergo epithelial–mesenchymal transition (EMT) under specific conditions such as exposure to TGF-β1,[24] menthol, and tobacco-flavored EC liquids or aerosols.[25] EMT is a key process of the metastatic spreading in which epithelial cells lose their cell polarity and cell–cell adhesion, and gain migratory and invasive properties.[26,27] Importantly, EMT can be triggered by FSS.[28] We applied the Hele-Shaw device to investigate the effect of FSS (τ_{cell} from 0.135 to 0.008 dyn cm^{-2}) on expression of vimentin, a key marker of the mesenchymal phenotype. To this end, the A549 VIM RFP cell line was used. This is a variant of the A549 cell line where vimentin is constitutively tagged with the red fluorescent protein, thereby enabling direct monitoring with confocal microscopy of the expression levels of this marker of the mesenchymal phenotype.[27,29] Vimentin expression decreased significantly from Section 1 (higher shear stress) to Section 5 (lower shear stress) of the device ($p = 0.02$) (**Figure 6**). Based on vimentin expression, EMT was triggered in A549 VIM RFP cells when exposed to shear stress above ≈0.03 dyn cm^{-2}. In addition, the morphology of the A549 VIM RFP cells changed noticeably along the sections of the Hele-Shaw channel, presenting more spindle-like than circular morphologies when exposed to higher shear stress and forming less dense monolayers than in the lower shear stress sections of the device.

Finally, we also confirmed that A549 VIM RFP cells cultured under a uniform FSS displayed uniform phenotype along the microfluidic culture channel. To this end, the A549 VIM RFP were grown within a constant-width device under high shear stress (0.15 dyn cm^{-2}). High expression of vimentin was imaged throughout the whole length of the channel. In addition, the A549 VIM RFP cells were cytokeratin negative, confirming the acquisition of a mesenchymal phenotype under this culture condition. Cell morphologies as imaged by high resolution confocal microscopy also confirmed the EMT with most cells displaying the characteristic spindle shape associated with this migratory and invasive phenotype (**Figure 7**).

2.4. Pumpless Cell Culture Device for Multiplexed Studies

Finally, we report on the design of a microfluidic device allowing the simultaneous application of different flow rates and

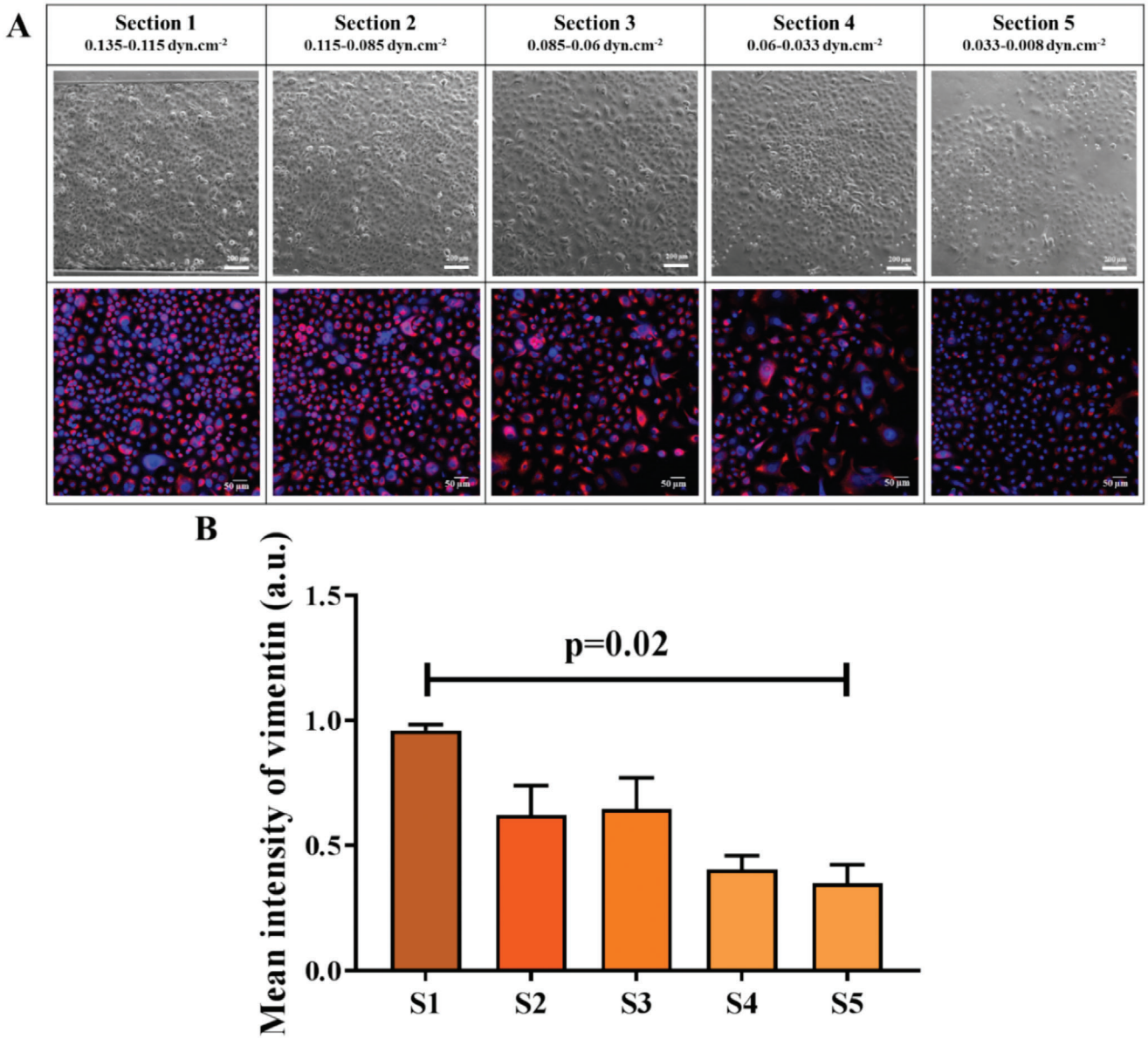

Figure 6. Epithelial to mesenchymal transition in A549 VIM RFP cells versus fluid shear stress in a Hele-Shaw device as indicated by vimentin expression. A) First row: Phase contrast images showing that confluent A549 cell monolayers are formed within 5 days. Bottom row: Confocal images showing vimentin expressions (red) in A549 cells. B) Mean fluorescence intensity (vimentin expression) in the different sections of the Hele-Shaw device corresponding to decreasing fluid shear stresses.

therefore FSS within a single chip. The device is designed to have five parallel channels which can be perfused with the same cell culture medium drawn from a common large rectangular reservoir in the inlet but under different flow rates driven by threads with different lengths (Figure S5A, Supporting Information SI5). We experimentally verified that different flow rates can be obtained in each channel by measuring nanoparticles velocity as described above (Figure S5B, Supporting Information SI5). We anticipate that this design provides a convenient methodology to test the influence of the shear stress experienced by cellular monolayers on their response to soluble factors.

3. Conclusion

Microfluidic organs-on-chips are rapidly becoming a mainstay technology for in vitro studies and are broadly anticipated to at least partially replace preclinical animal models. Toward facilitating their implementation in laboratories with no or limited experience and facilities in microfluidics, we here developed a new pumpless organ-on-chip approach that enables autonomous perfusion of cellular monolayers. The perfusion within PDMS/glass-based microfluidic devices is driven by the controlled evaporation of medium or buffer wicking superhydrophilic fibers positioned in the outlet. The flow rate within the pumpless devices can be

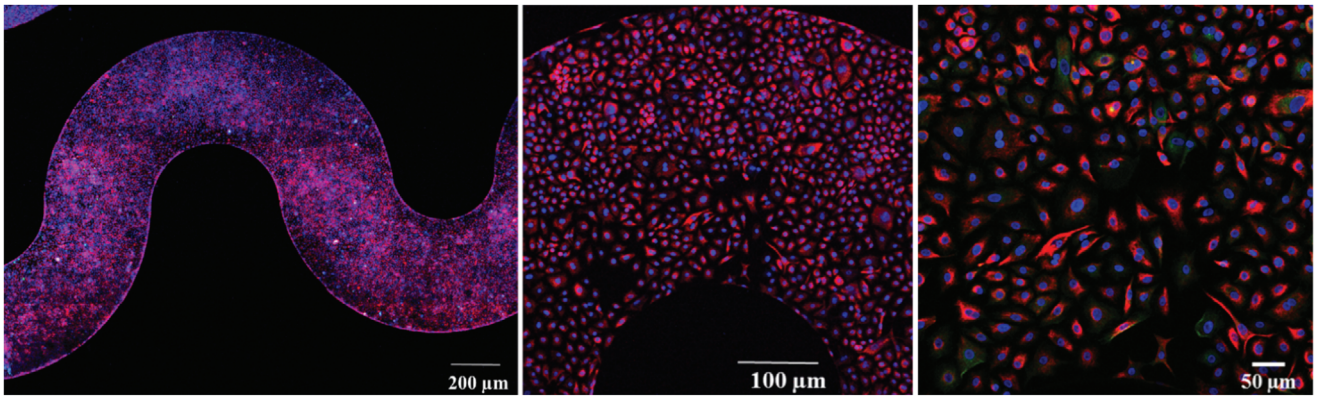

Figure 7. Epithelial to mesenchymal transition in A549 VIM RFP cells induced by high fluid shear stress. Vimentin (red) and cytokeratin (green) expressions in A549 VIM RFP cells cultured for 5 days under a flow rate of 0.3 µL min^{-1} (corresponding to 0.15 dyn cm^{-2}).

easily adjusted by changing the diameter and length of the thread. Caco-2 cells monolayers cultured within the pumpless device displayed similar characteristics as monolayers cultured using standard high-precision pumps. We also applied this approach to investigate the role of the FSS on A549 cells phenotype and demonstrated that they adopt mesenchymal phenotypes when cultured above 0.03 dyn cm^{-2}. The pumpless device is completely equipment free, versatile, and easy to use. The absence of tubings also enable to maintain the whole device within a sterile Petri dish, which greatly reduces the risk of contamination. A limitation of this approach is that very high flow rates cannot be realized, therefore limiting its application to organs-on-chips models based on cell types that do not require high applied shear stress. Nevertheless, we anticipate that their application could facilitate the preparation of organs-on-chips by non-specialist users, including for primary cells and patient-derived organoids.

4. Experimental Section

Device Fabrication: All devices were fabricated using standard soft lithography and consisted of single or multiple fluidic polydimethylsiloxane (PDMS) channels, bonded to glass coverslips (Proscitech, G418, No1). Briefly, SU-8 photoresist 50 was spun using a Karl Suss Delta 80 spin coater (Suss MicroTec, Germany) to produce a 150 µm layer (2000 rpm spin) on a silicon wafer. The master molds were created with a Dilase 650 mask writer (Kloe, France), followed by the development and thermal hardening of the SU-8. A 10 mm thick PDMS layer (10:1, w/w) was cast onto the master mold and cured for 2 h at 65 °C. It was cut and peeled off, then punched to create a hole (e.g., 8 mm) for the inlet reservoir while a 1.5 mm hole was punched to serve as the outlet. This smaller hole enables the placement of the thread within the outlet but without contacting the bottom glass substrate (see Figure 1). The PDMS layer was then oxygen plasma treated and bound to a glass coverslip for at least 10 min at 65 °C to produce permanent bonding. Three different microfluidic devices were used to validate the proposed "pumpless approach," namely a constant-width channel device, a Hele-Shaw device which allows to apply a range of shear stresses along the FSS axis[4,17] (Figure S3, Supporting Information SI1), and a multiplex device with five parallel microchannels (Figure S5).

Spunlace (70% rayon, 30% polyester, from Ebos Healthcare Australia) superhydrophilic threads (wet and dry tensile strength 45 g m^{-2} fabric) were used to drive the flow within the microfluidic devices. To activate the flow of culture medium or buffer, a thread was inserted in the outlet hole within the PDMS (Figure 1). In this configuration, evaporation of the liquid wicking the thread provides the driving force to achieve continuous flow within the channel. A small lid was placed at the inlet reservoir to prevent evaporation of the medium (see Figure 1). The length of the thread was adjusted depending on the flow rate required for a specific cell type. The complete devices were placed in sterile 92 × 16 mm Petri dishes (Sarstedt) and kept in an incubator as described below.

Characterization of Threads: Threads were imaged on an adhesive carbon disc using a benchtop SEM (JEOL Neoscope (JCM-5000)) with an acceleration of 2 kV (Figure 2). To determine the capillary properties of the superhydrophilic thread, four different diameters of thread were tested (0.5, 1, 1.5, and 2 mm). Briefly, 10 cm thread lengths were dipped into a dye solution and the levels (wicking heights) of the dye was measured over time.

Characterization of Thread-Driven Flow Rate: The flow behavior induced within the microfluidic channel by a thread of specific characteristics was verified experimentally by measuring the velocity of highly fluorescent nanoparticles. The motion of 200 nm polystyrene beads (FluoSpheres, Thermo Fisher) within a constant-width channel was monitored with an inverted Eclipse Ti-E Nikon microscope (Nikon, Japan) equipped with an ANDOR zyla 5.5 camera (Andor Technology Ltd., Belfast Northern Ireland) using 20× objective. The NIS-Elements BR (Nikon, Japan) software and Icecream App were used for screen recording. The average flow rate was approximated using Equation (1).

$$Q_{\text{fluid}} = V_{\text{particles}} \times A_{\text{channel}} \quad (1)$$

With Q_{fluid} the flow rate (µL min^{-1}); A_{channel} the cross-sectional area of the channel (0.15 mm^2 in this study), and $V_{\text{particles}}$ the averaged velocities of three particles in three different areas (nine particles in total) in the middle of the channel (in mm min^{-1}). Each experiment was repeated three times. Low flow rates (<1 µL min^{-1}) were established by placing shorter threads straight out from the outlet while high flow rates (>1 µL min^{-1}) were achieved by bending the thread out of the outlet.

Pumpless Culture of Caco-2 and A549 Cells: Human intestinal epithelial Caco-2 cells (Caco-2 BBE human colorectal carcinoma line, ATCC CRL-2102)[18] were cultured in 75 cm^2 tissue culture flasks in Dulbecco's Modified Eagle Medium (DMEM, Sigma-Aldrich, Australia) F-12 Ham supplemented with 10% fetal bovine serum (FBS) (Life Technologies), 1% L-glutamine (Sigma-Aldrich), and 1% streptomycin/penicillin (Sigma-Aldrich) at 37 °C and at 5% CO_2 levels in a humidifying incubator. Human lung epithelial A549 cells (ATCC CCL-185 human lung carcinoma line)[19] were cultured in 75 cm^2 tissue culture flasks in DMEM F12-K mixture (Gibco, Thermo Fisher, Australia) supplemented with 10% FBS, 1% L-glutamine, and 1% streptomycin/penicillin at 37 °C and at 5% CO_2 levels in a humidifying incubator. The A549 VIM RFP cell line was also used (ATCC CCL-185EMT) to enable direct imaging of vimentin expression.

Before seeding the devices, the channels were treated with 70% v/v ethanol and then washed with cold phosphate buffered saline (PBS, Ca^{2+}

and Mg^{2+} free, pH = 7.4, Sigma-Aldrich), each for 30 min at room temperature (RT) in a biosafety hood. Each device was then transferred to a sterile Petri dish. A cold 1% v/v Matrigel basement membrane matrix solution (FAL354234, Corning, BD Biosciences, Tewksbury, MA, USA) in serum-free culture medium was then injected within the device from the outlet and left to incubate for 1 h at 37 °C under static conditions to coat the glass coverslip surface. Cells were harvested with 0.25% trypsin/EDTA (Sigma-Aldrich) and pipetted inside the device from the outlet to avoid cell loss in the relatively large inlet reservoir. A concentration of 2×10^5 cells per cm^2 was used and the cells were left to adhere to the Matrigel coated glass for at least 1 h. The total area of the surface area for the constant-width channel was 0.35 cm^2 and the total volume was 5.25 µL. The total area of the Hele-Shaw channel was 2.552 cm^2 and the total volume was 38.28 µL. Following cell attachment, cell culture medium was added in the inlet reservoir to gently flush the channel and remove unattached cells. A thread was then inserted in the outlet as described above. The cell medium flow rate post attachment for the constant-width channel was set at 0.15 µL min^{-1}, and for the Hele-Shaw chamber at 0.22 µL min^{-1} for Caco-2 cells. This corresponded in the device used here to an applied shear stress of 0.02 dyn cm^{-2} in the constant-width channels. The Caco-2 cells were grown for 5 days to form a confluent and fully differentiated monolayer, as previously described.[20] In the design used in this study, the inlet reservoir was defined in the PDMS slab and had a diameter of 8 mm. The inlet reservoir was refilled everyday with ≈200 µL of fresh cell culture medium. The cell density was monitored daily using bright field microscopy on an inverted Eclipse Ti-E Nikon microscope (Nikon, Japan). A549 cells were cultured under higher flow rates corresponding to higher shear stress values (e.g., 0.075 dyn cm^{-2} in the constant-width channel). Indeed, intestinal cells (like Caco-2 cell line) are known to proliferate and differentiate well under low shear in such devices (≈0.005–0.025 dyn cm^{-2}),[4] while lung cells such as the A549 cell line have been shown to undergo EMT upon culture under moderate shear stress (up to 30 dyn cm^{-2}).[5,21] The values of flow rates and shear stresses used in this study are summarized in Table 1 and in Figure S4, Supporting Information SI4 for the Hele-Shaw device. Note that the shear stress is the one experienced by the cells (τ_{cell}).

Characterization of Monolayers Cultured in Pumpless Organ-on-Chip Devices: Phase contrast images were captured with an inverted Eclipse Ti-E microscope (Nikon) equipped with an ANDOR zyla 5.5 camera (Andor Technology Ltd) at 10× and 20× magnifications and using the NIS-Elements BR (Nikon, Japan) software. Phase contrast was used to qualitatively image the density of vacuoles as well as the proliferation of the cells over time within the devices (Figure S1, Supporting Information SI2) while cells were alive. All immunofluorescence imaging was performed on cellular monolayers fixed with 4% w/v formaldehyde. Cells were permeabilized with 0.1% v/v Triton X-100 for 15 min before blocking with 5% w/v bovine serum albumin (BSA) for 1 h on ice and then washing with PBS (all from Sigma-Aldrich, Australia). Fixed monolayers were sequentially incubated at 4 °C overnight with primary antibodies in 1% BSA at the following concentrations: anti-Zona Occludens (ZO)-1 (mouse monoclonal, Thermo Fisher Scientific, # 33–9100) at 2 µg mL^{-1}, anti-Mucin 2 (Muc2) (polyclonal rabbit, Abcam, ab76774) at 2 µg mL^{-1} and FITC-conjugated anti-pan cytokeratin (MACS, Clone REA831, 130-112-931) at 1 µg mL^{-1}. Corresponding secondary antibodies were then used: AlexaFluor 488-conjugated goat anti-mouse IgG (Abcam) at 1 µg mL^{-1}, AlexaFluor 647-conjugated goat anti-rabbit IgG (Sigma-Aldrich) at 1 µg mL^{-1} in PBS for 2 h at RT. Monolayers were finally incubated with 4′,6-diamidino-2-phenylindole dihydrochloride (DAPI) at 0.1 µg mL^{-1} (Sigma-Aldrich) for nuclei staining. To visualize F-actin, 20 µg mL^{-1} of FITC-Phalloidin (Sigma-Aldrich) was applied at RT for 40 min. To visualize mitochondria, 500 nM of MitoTraker Deep Red FM (Thermo Fisher Scientific) was perfused for 45 min in the devices at RT before fixation of the monolayers. All solutions were perfused in the devices at ≈5 µL min^{-1} using a sterile tissue placed in contact with the thread.

Monolayers were imaged with a LSM 710 confocal microscope (Zeiss, Germany) equipped with a sCMOS PCO Edge camera using either a 10×, 20× objective or an immersion oil objective 63× with water immersion. Imaging was performed in random area within the constant-width devices and along the *z* axis of the Hele-Shaw channel as described previously.[4] Three images for each defined section (every cm) were randomly taken (this was repeated at least $n = 3$ independent devices). The mean fluorescence intensities for vimentin and cytokeratin (for A549 cells) were measured using ImageJ (NIH). The acquired 16-bit grey scale images were analyzed with ImageJ to calculate the pixel intensity normalized per unit of area (mean pixel intensity per unit area divided by maximum intensity of the images).[22] For evaluating the height of a monolayer using F-actin staining, five measurements at random positions were performed using ImageJ in two images for each section taken from each of the three independent experiments (Figure S2, Supporting Information SI2).

Statistics: Data presented are the mean ± standard error of mean from three assays in a given type of device (constant width or Hele-Shaw). A Kruskal–Wallis test (non-parametric one-way analysis of variance) was performed except if indicated. The difference between each group was then compared with the Dunn's test. All statistical data analysis was performed with GraphPad Prism 7.04 for Windows (GraphPad Prism Software, La Jolla, CA). A p-value < 0.05 was validating a statistically significant difference between groups.

Supporting Information

Supporting Information is available from the Wiley Online Library or from the author.

Acknowledgements

The authors acknowledge funding from the Australian Research Council Linkage Grant LP150100032 and the Australian Research Council Centre of Excellence in Convergent Bio-Nano Science and Technology. This work was performed in part at the South Australian node of the Australian National Fabrication Facility under the National Collaborative Research Infrastructure Strategy to provide nano- and microfabrication facilities for Australia's researchers. The authors acknowledge the facilities, scientific, and technical assistance of NCRIS and Microscopy Australia at the University of South Australia, a facility that is co-funded by the University of South Australia, the State and Federal Governments. The authors would like to thank Nobuyuki Kawashima for SEM imaging.

Conflict of Interest

The authors declare no conflict of interest.

Author Contributions

L.C.D. and A.N. contributed equally to this work. L.C.D., A.N., E.C., C.P., and B.T. conceived and designed the study and approved the manuscript. L.C.D, A.N, and E.C. performed the experiments and analyzed the data. L.C.D. and A.N. wrote the manuscript.

Keywords

adenocarcinomic human alveolar basal epithelial A549 cells, human epithelial colorectal adenocarcinoma cells Caco-2 cells, microfluidic devices, organ-on-chip, pumpless devices, superhydrophilic, tubeless devices

Received: December 13, 2019
Revised: March 5, 2020
Published online: April 28, 2020

[1] a) B. Zhang, A. Korolj, B. F. L. Lai, M. Radisic, *Nat. Rev. Mater.* **2018**, *3*, 257; b) E. W. Esch, A. Bahinski, D. Huh, *Nat. Rev. Drug Discovery* **2015**, *14*, 248.
[2] B. Ladoux, R.-M. Mege, *Nat. Rev. Mol. Cell Biol.* **2017**, *18*, 743.
[3] R. S. Reneman, T. Arts, A. P. Hoeks, *J. Vasc. Res.* **2006**, *43*, 251.
[4] L. C. Delon, Z. Guo, A. Oszmiana, C. C. Chien, R. Gibson, C. Prestidge, B. Thierry, *Biomaterials* **2019**, *225*, 119521.
[5] E. W. Flitney, E. R. Kuczmarski, S. A. Adam, R. D. Goldman, *FASEB J.* **2009**, *23*, 2110.
[6] D. Huh, B. D. Matthews, A. Mammoto, M. Montoya-Zavala, H. Y. Hsin, D. E. Ingber, *Science* **2010**, *328*, 1662.
[7] H. J. Kim, D. Huh, G. Hamilton, D. E. Ingber, *Lab Chip* **2012**, *12*, 2165.
[8] S. A. Lee, E. Kang, J. Ju, D. S. Kim, S. H. Lee, *Lab Chip* **2013**, *13*, 3529.
[9] F. Zheng, F. Fu, Y. Cheng, C. Wang, Y. Zhao, Z. Gu, *Small* **2016**, *12*, 2253.
[10] M. Komeya, K. Hayashi, H. Nakamura, H. Yamanaka, H. Sanjo, K. Kojima, T. Sato, M. Yao, H. Kimura, T. Fujii, T. Ogawa, *Sci. Rep.* **2017**, *7*, 15459.
[11] H. J. Chen, P. Miller, M. L. Shuler, *Lab Chip* **2018**, *18*, 2036.
[12] S. J. Trietsch, E. Naumovska, D. Kurek, M. C. Setyawati, M. K. Vormann, K. J. Wilschut, H. L. Lanz, A. Nicolas, C. P. Ng, J. Joore, S. Kustermann, *Nat. Commun.* **2017**, *8*, 262.
[13] H. E. Abaci, K. Gledhill, Z. Guo, A. M. Christiano, M. L. Shuler, *Lab Chip* **2015**, *15*, 882.
[14] H. Lee, D. S. Kim, S. K. Ha, I. Choi, J. M. Lee, J. H. Sung, *Biotechnol. Bioeng.* **2017**, *114*, 432.
[15] M. Marimuthu, S. Kim, *Anal. Biochem.* **2013**, *437*, 161.
[16] A. Nilghaz, S. Hoo, W. Shen, X. Lu, P. P. Chan, *Sens. Actuators, B* **2018**, *257*, 650.
[17] S. Usami, H. H. Chen, Y. Zhao, S. Chien, R. Skalak, *Ann. Biomed. Eng.* **1993**, *21*, 77.
[18] M. D. Peterson, M. S. Mooseker, *J. Cell Sci.* **1992**, *102*, 581.
[19] K. A. Foster, C. G. Oster, M. M. Mayer, M. L. Avery, K. L. Audus, *Exp. Cell Res.* **1998**, *243*, 359.
[20] K. Pocock, L. Delon, V. Bala, S. Rao, C. Priest, C. A. Prestidge, B. Thierry, *ACS Biomater. Sci. Eng.* **2017**, *3*, 951.
[21] A. Jaitovich, S. Mehta, N. Na, A. Ciechanover, R. D. Goldman, K. M. Ridge, *J. Biol. Chem.* **2008**, *283*, 25348.
[22] C. A. Schneider, W. S. Rasband, K. W. Eliceiri, *Nat. Methods* **2012**, *9*, 671.
[23] K. Pocock, L. C. Delon, A. Khatri, C. Prestidge, R. Gibson, C. Barbe, B. Thierry, *Biomater. Sci.* **2019**, *7*, 2410.
[24] V. Tirino, R. Camerlingo, K. Bifulco, E. Irollo, R. Montella, F. Paino, G. Sessa, M. V. Carriero, N. Normanno, G. Rocco, G. Pirozzi, *Cell Death Dis.* **2013**, *4*, e620.
[25] A. Zahedi, R. Phandthong, A. Chaili, G. Remark, P. Talbot, *Lung Cancer* **2018**, 122.
[26] J. P. Thiery, H. Acloque, R. Y. Huang, M. A. Nieto, *Cell* **2009**, *139*, 871.
[27] R. Kalluri, R. A. Weinberg, *J. Clin. Invest.* **2009**, *119*, 1420.
[28] S. Liu, F. Zhou, Y. Shen, Y. Zhang, H. Yin, Y. Zeng, J. Liu, Z. Yan, X. Liu, *Oncotarget* **2016**, *7*, 32876.
[29] M. G. Mendez, S. I. Kojima, R. D. Goldman, *FASEB J.* **2010**, *24*, 1838.